J|A|C|S
ARTICLES
Published on Web 03/30/2004

Photoelectron Spectroscopy of the Doubly-Charged Anions $[M^{IV}O(mnt)_2]^{2-}$ (M = Mo, W; mnt = $S_2C_2(CN)_2^{2-}$): Access to the Ground and Excited States of the $[M^{V}O(mnt)_2]^{-}$ Anion

Tom Waters,[†] Xue-Bin Wang,[‡] Xin Yang,[‡] Lianyi Zhang,[†,§] Richard A. J. O'Hair,[†] Lai-Sheng Wang,*[,‡] and Anthony G. Wedd*[,†]

Contribution from the School of Chemistry, The University of Melbourne, Victoria, Australia, 3010, the Department of Physics, Washington State University, Richland, Washington 99352, and the W. R. Wiley Environmental Molecular Sciences Laboratory, Pacific Northwest National Laboratory, Richland, Washington 99352

Received November 18, 2003; E-mail: ls.wang@pnl.gov; agw@unimelb.edu.au

Abstract: Photodetachment photoelectron spectroscopy was used to investigate the electronic structure of the doubly charged complexes $[M^{IV}O(mnt)_2]^{2-}$ (M = Mo, W; mnt = 1,2-dicyanoethenedithiolato). These dianions are stable in the gas phase and are minimal models for the active sites of the dimethyl sulfoxide reductase family of molybdenum enzymes and of related tungsten enzymes. Adiabatic and vertical electron binding energies for both species were measured, providing detailed information about molecular orbital energy levels of the parent dianions as well as the ground and excited states of the product anions $[M^{V}O(mnt)_2]^{-}$. Density functional theory calculations were used to assist assignment of the detachment features. Differences in energy between these features provided the energies of ligand-to-metal charge-transfer transitions from S(π) and S(σ) molecular orbitals to the singly occupied metal-based orbital of the products $[M^{V}O(mnt)_2]^{-}$. These unique data for the M^{V} species were obtained at the C_{2v} geometry of the parent M^{IV} dianions. However, theoretical calculations and available condensed phase data suggested that a geometry featuring differentially folded dithiolene ligands (C_s point symmetry) was slightly lower in energy. The driving force for ligand folding is a favorable covalent interaction between the singly occupied metal-based molecular orbital (a_1 in C_{2v} point symmetry; highest occupied molecular orbital (HOMO)) and the least stable of the occupied sulfur-based molecular orbitals (b_1 in C_{2v} point symmetry, HOMO−1) that is only possible upon reduction to the lower symmetry. This ligand folding induces a large increase in the intensity predicted for the a′ S(π) → a′ $d_{x^2-y^2}$ charge-transfer transition originating from the HOMO−2 of $[M^{V}O(mnt)_2]^{-}$ under C_s point symmetry. Electronic absorption spectra are available for the related species $[Mo^{V}O(bdt)_2]^{-}$ (bdt = 1,2-benzenedithiolato) and for the oxidized form of dimethyl sulfoxide reductase. The intense absorptions at ~1.7 eV have been assigned previously to S(σ) → Mo transitions, assuming C_{2v} geometry. The present work indicates that the alternative a′ S(π) → a′ $d_{x^2-y^2}$ of C_s geometry must be considered. Overall, this study confirms that the electronic structure of the M-dithiolene units are exquisitely sensitive to dithiolene ligand folding, reinforcing the proposal that these units are tunable conduits for electron transfer in enzyme systems.

Introduction

Mononuclear molybdenum- and tungsten-containing enzymes catalyze a number of two-electron redox processes that contribute to the global metabolism of carbon, nitrogen, and sulfur.[1−3] These reactions appear to proceed by formal oxygen atom transfer and coupled electron−proton-transfer steps, with the metals cycling through M(VI,V,IV) oxidation states during turnover. The molybdenum enzymes may be divided into three principal families (sulfite oxidase, xanthine oxidase, and dimethyl sulfoxide reductase) on the basis of catalytic function and structural homology at the active site.[2,4] Crystal structures reveal the presence of either one or two pyranopterin units (Structure I) coordinated to the metal center through the ene-1,2-dithiolato (dithiolene) moiety.[5]

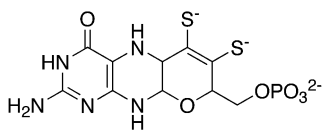

I (phosphate form)

Synthetic analogues have been developed to mimic the active sites of these enzymes with the aim of understanding their

[†] The University of Melbourne.
[‡] Washington State University and Pacific Northwest National Laboratory.
[§] Visiting scientist (2000−2001) from Xinjiang Agricultural University, Xinjiang, P. R. China.

(1) *Molybdenum and Tungsten, Their Roles in Biological Processes*; Sigel, A., Sigel, H., Eds.; Metal Ions in Biological Systems 39; Marcel Dekker: New York, 2002.
(2) Hille, R. *Chem. Rev.* **1996**, *96*, 2757−2816.
(3) Johnson, M. K.; Rees, D. C.; Adams, M. W. W. *Chem. Rev.* **1996**, *96*, 2817−2839.

structural, chemical, and spectroscopic properties.[6−9] Structural models for the dimethyl sulfoxide reductase family incorporate two dithiolene ligands and oxo and/or XR (X = O, S, Se) ligands, the latter to mimic serinyl, cysteinyl, and selenocysteinyl ligation. Examples include oxomolybdenum(IV/V)-, dioxomolybdenum(VI)-, and aryloxo- or siloxo-molybdenum(IV)-bis(dithiolene) centers.[10−17] Tungsten versions have also been reported in the context of the aldehyde:ferredoxin oxidoreductase and formate dehydrogenase enzymes and allow a direct comparison of properties with their molybdenum counterparts.[18−22] Related vanadium-containing species have also been prepared.[23,24]

The electronic structures of a range of $[Mo^{V}OS_4]^-$ (d^1) species (S_4 = tetrathiolato, bis(dithiolato), or bis(dithiolene)) have been investigated by a combination of physical and theoretical techniques.[25−32] Intense low-energy transitions in electronic spectra are proposed to involve charge transfer from molecular orbitals of predominantly ligand sulfur character to the highest occupied molecular orbital (HOMO), which is metal-based and essentially nonbonding.[27−31]

Photodetachment photoelectron spectroscopy (PES) allows detailed investigation of the electronic structure of gaseous species. In addition to providing ionization energies and electron affinities, the technique can also provide information about excited states of the ionized molecule. When applied to species that are involved in electron transfer or redox reactions, photodetachment experiments allow investigation of the intrinsic oxidation energy, as well as relaxation or reorganization energies associated with a redox event. In select cases, geometries closely resembling those of a transition state can be investigated.[33] This is possible when the geometry of the parent species corresponds closely to that of a transition state on the potential energy surface of the product species generated by electron detachment.

A number of relevant molybdenum systems have been investigated by photoelectron spectroscopy.[32,34−37] A majority involved neutral molecules that required sublimation for transfer to the gas phase, thereby limiting experiments to systems of sufficient volatility and/or thermal stability. However, electrospray ionization (ESI) allows charged species to be transferred directly from the solution to the gaseous phase and is particularly suited to species that exist as preformed ions in solution.[38] The coupling of an electrospray ionization source to a photoelectron spectrometer[39] has allowed a number of negatively charged inorganic species to be investigated for the first time.[40−43] The technique was applied recently to a series of oxo-molybdenum(V)-tetrathiolato and -bis(dithiolene) anions $[Mo^{V}OS_4]^-$ that represent simple models for the metal coordination environment of DMSO reductase.[32]

The present study describes the use of ESI to transfer $[M^{IV}O(mnt)_2]^{2-}$ (M = Mo, W; mnt = $[S_2C_2(CN)_2]^{2-}$; maleonitriledithiolate or 1,2-dicyanoethenedithiolate) dianions to the gas phase where they were studied by photodetachment photoelectron spectroscopy. The electron-withdrawing cyanide substituents were chosen to ensure that these species exhibit positive electron affinities and were stable dianions in the gas phase.[44] Experimental data were interpreted with the aid of density functional theory (DFT) calculations on the ground states of the parent anions as well as on the ground and excited states of the product anions. The experiments provided insights into the energetics of ligand-to-metal charge transfer that are common to $[Mo^{V}OS_4]^-$ centers, providing data that are complementary to those obtained for related species by other techniques. As a consequence of the vertical nature of electron detachment from $[M^{IV}O(mnt)_2]^{2-}$, these data were accessed at a well-defined geometry of $[Mo^{V}O(mnt)_2]^-$ with equivalent dithiolene ligands (C_{2v} point symmetry). The effect of variation

(4) Hille, R. Molybdenum Enzymes Containing the Pyranopterin Cofactor: An Overview. In ref 1; pp 187−226.
(5) Dobbek, H.; Huber, R. The Molybdenum and Tungsten Cofactors: A Crystallographic View. In ref 1; pp 227−263.
(6) Young, C. G.; Wedd, A. G. *Chem. Commun.* **1997**, 1251−1257.
(7) Young, C. G. Biomimetic Chemistry of Molybdenum. In *Biomimetic Oxidations Catalyzed by Transition Metal Complexes*; Meunier, B., Ed.; Imperial College Press: London, **2000**; pp 415−459.
(8) Fischer, B.; Burgmayer, S. J. N. Models for the Pyranopterin-Containing Molybdenum and Tungsten Cofactors. In ref 1; pp 265−316.
(9) Enemark, J. H.; Cooney, J. J. A.; Wang, J.-J.; Holm, R. H. *Chem. Rev.* **2004**, *104*, 1175−1200.
(10) Boyde, S.; Ellis, S. R.; Garner, C. D.; Clegg, W. *Chem. Commun.* **1986**, 1541−1543.
(11) Donahue, J. P.; Goldsmith, C. R.; Nadiminti, U.; Holm, R. H. *J. Am. Chem. Soc.* **1998**, *120*, 12869−12881.
(12) Lim, B. S.; Donahue, J. P.; Holm, R. H. *Inorg. Chem.* **2000**, *39*, 263−273.
(13) Davies, E. S.; Beddoes, R. L.; Collison, D.; Dinsmore, A.; Docrat, A.; Joule, J. A.; Wilson, C. R.; Garner, C. D. *J. Chem. Soc., Dalton Trans.* **1997**, 3985−3995.
(14) Oku, H.; Ueyama, N.; Nakamura, A. *Chem. Lett.* **1995**, 621−622.
(15) Oku, H.; Ueyama, N.; Kondo, M.; Nakamura, A. *Inorg. Chem.* **1994**, *33*, 209−216.
(16) Ueyama, N.; Oku, H.; Kondo, M.; Okamura, T.-A.; Yoshinaga, N.; Nakamura, A. *Inorg. Chem.* **1996**, *35*, 643−650.
(17) Das, S. K.; Chaudhury, P. K.; Biswas, D.; Sarkar, S. *J. Am. Chem. Soc.* **1994**, *116*, 9061−9070.
(18) Das, S. K.; Biswas, D.; Maiti, R.; Sarkar, S. *J. Am. Chem. Soc.* **1996**, *118*, 1387−1397.
(19) Ueyama, N.; Oku, H.; Nakamura, A. *J. Am. Chem. Soc.* **1992**, *114*, 7310−7311.
(20) Lorber, C.; Donahue, J. P.; Goddard, C. A.; Nordlander, E.; Holm, R. H. *J. Am. Chem. Soc.* **1998**, *120*, 8102−8112.
(21) Davies, E. S.; Aston, G. M.; Beddoes, R. L.; Collison, D.; Dinsmore, A.; Docrat, A.; Joule, J. A.; Wilson, C. R.; Garner, C. D. *J. Chem. Soc., Dalton Trans.* **1998**, 3647−3656.
(22) Sung, K.-M.; Holm, R. H. *Inorg. Chem.* **2001**, *40*, 4518−4525.
(23) Cooney, J. J. A.; Carducci, M. D.; McElhaney, A. E.; Selby, H. D.; Enemark, J. H. *Inorg. Chem.* **2002**, *41*, 7086−7093.
(24) Collison, D.; Mabbs, F. E.; Temperley, J.; Christou, G.; Huffman, J. C. *J. Chem. Soc., Dalton Trans.* **1988**, 309−314.
(25) Hanson, G. R.; Brunette, A. A.; McDonell, A. C.; Murray, K. S.; Wedd, A. G. *J. Am. Chem. Soc.* **1981**, *103*, 1953−1959.
(26) Oku, H.; Koehler, B. P.; Ueyama, N.; Nakamura, A.; Johnson, M. K. *J. Inorg. Biochem.* **1997**, *67*, 14.
(27) McNaughton, R. L.; Helton, M. E.; Rubie, N. D.; Kirk, M. L. *Inorg. Chem.* **2000**, *39*, 4386-4387.
(28) McNaughton, R. L.; Tipton, A. A.; Rubie, N. D.; Conry, R. R.; Kirk, M. L. *Inorg. Chem.* **2000**, *39*, 5697−5706.
(29) McMaster, J.; Carducci, M. D.; Yang, Y.-S.; Solomon, E. I.; Enemark, J. H. *Inorg. Chem.* **2001**, *40*, 687−702.
(30) Helton, M. E.; Gebhart, N. L.; Davies, E. S.; McMaster, J.; Garner, C. D.; Kirk, M. L. *J. Am. Chem. Soc.* **2001**, *123*, 10389−10390.
(31) Basu, P.; Nemykin, V. N.; Sengar, R. S. *Inorg. Chem.* **2003**, *42*, 7489−7501.
(32) Wang, X.-B.; Inscore, F. E.; Yang, X.; Cooney, J. J. A.; Enemark, J. H.; Wang, L.-S. *J. Am. Chem. Soc.* **2002**, *124*, 10182−10191.
(33) See, for example: (a) Manolopoulos, D. E.; Stark, K.; Werner, H. J.; Arnold, D. W.; Bradforth, S. E.; Neumark, D. M. *Science* **1993**, *262*, 1852−1855. (b) Neumark, D. *Acc. Chem. Res.* **1993**, *26*, 33−40. (c) Wenthold, P. G.; Hrovat, D. A.; Borden, W. A.; Lineberger, W. C. *Science* **1996**, *272*, 1456−1459. (d) Wenthold, P. G.; Lineberger, W. C. *Acc. Chem. Res.* **1999**, *32*, 597−604.
(34) Westcott, B. L.; Gruhn, N. E.; Enemark, J. H. *J. Am. Chem. Soc.* **1998**, *120*, 3382−3386.
(35) Helton, M. E.; Gruhn, N. E.; McNaughton, R. L.; Kirk, M. L. *Inorg. Chem.* **2000**, *39*, 2273−2278.
(36) Joshi, H. K.; Inscore, F. E.; Schirlin, J. T.; Dhawan, I. K.; Carducci, M. D.; Bill, T. G.; Enemark, J. H. *Inorg. Chim. Acta* **2002**, *337*, 275−286.
(37) Joshi, H. K.; Cooney, J. J. A.; Inscore, F. E.; Gruhn, N. E.; Lichtenberger, D. L.; Enemark, J. H. *Proc. Natl. Acad. Sci. U.S.A.* **2003**, *100*, 3719−3724.
(38) Traeger, J. C. *Int. J. Mass Spectrom.* **2000**, *200*, 387−401.
(39) Wang, L. S.; Ding, C. F.; Wang, X. B.; Barlow, S. E. *Rev. Sci. Instrum.* **1999**, *70*, 1957−1966.
(40) Wang, X. B.; Wang, L. S. *J. Chem. Phys.* **1999**, *111*, 4497−4509.
(41) Wang, X. B.; Wang, L. S. *J. Am. Chem. Soc.* **2000**, *122*, 2096−2100.
(42) Wang, X. B.; Vorpagel, E. R.; Yang, X.; Wang, L. S. *J. Phys. Chem. A* **2001**, *105*, 10468−10474.
(43) Yang, X.; Razavet, M.; Wang, X. B.; Pickett, C. J.; Wang, L. S. *J. Phys. Chem. A* **2003**, *107*, 4612−4618.

in conformation of the dithiolene ligand (fold angle) upon the electronic structure of such centers was examined theoretically and compared with available experimental data.

Experimental Details

Synthesis. $(Bu_4N)_2[M^{IV}O(mnt)_2]$ and $(Et_4N)_2[W^{IV}O(mnt)_2]$ were prepared by literature methods.[17,18]

Photodetachment Photoelectron Spectroscopy. The design and operation of the ESI−PES apparatus has been described in detail, and a brief description only is provided here.[39] The desired anions $[M^{IV}O(mnt)_2]^{2-}$ were generated by electrospraying 10^{-3} M solutions of $(Bu_4N)_2[M^{IV}O(mnt)_2]$ or $(Et_4N)_2[W^{IV}O(mnt)_2]$ in CH_3CN solvent. The solutions were sprayed from a 0.01-mm diameter syringe needle biased at −2.2 kV into a desolvation capillary maintained at ∼70 °C. Negative ions emerging from this capillary were transferred into a quadrupole ion trap and accumulated for a period of 100 ms, before being passed into the extraction zone of a time-of-flight mass spectrometer. Anions of interest were mass-selected and decelerated before being intercepted by a laser beam in the detachment zone of a magnetic bottle PES analyzer. In the present study, 355 nm (3.496 eV) and 266 nm (4.661 eV) photons from a Q-switched Nd:YAG laser and 193 nm (6.424 eV) and 157 nm (7.866 eV) photons from an excimer laser were used for photodetachment. Photoelectrons were collected at nearly 100% efficiency by the magnetic bottle and analyzed in a 4-m photoelectron tube. Photoelectron time-of-flight spectra were converted to kinetic energy spectra and calibrated with the known spectra of I^- and O^-. Binding energy spectra were calculated by subtracting the kinetic energy spectra from the known photon energies. Energy resolution ($\Delta E/E$) was estimated as approximately 2% (fwhm), i.e., about 10 meV for 0.5 eV electrons, as measured from the spectra of I^- at 355 nm.

Due to the lack of vibrational resolution, adiabatic detachment energies (ADEs) were measured by drawing a straight line along the leading edge of the threshold band and then adding a constant to the intersection with the binding energy axis to take into account the finite resolution and a thermal broadening. These were determined from the 355-nm spectra for each complex because of the better resolution at the lower photon energy. The vertical detachment energy (VDE) of each peak was measured straightforwardly from the peak maximum.

Theoretical Methods. DFT calculations employing the hybrid B3LYP functional were carried out using the Gaussian 98 program.[45] Molecular orbitals were visualized using the Molden package.[46] Calculations on $[M^{IV}O(mnt)_2]^{2-}$ and $[M^{V}O(mnt)_2]^-$ were carried out using the 6-31$^+$G* basis set for C, N, O, and S and the effective core potential basis sets of Stevens et al. for Mo and W.[47] The same basis sets were used for calculations on $[M^{V}O(bdt)_2]^-$ (bdt = 1,2-benzenedithiolato), except the 6-31G* basis set was used for H and C. The geometries of the singlet dianions $[M^{IV}O(mnt)_2]^{2-}$ were optimized under constrained C_{2v} point symmetry in spin-restricted mode (RB3LYP). The geometry of the doublet anions $[M^{V}O(mnt)_2]^-$ and $[M^{V}O(bdt)_2]^-$ were optimized under constrained C_{2v} or C_s point symmetry in spin-unrestricted mode (UB3LYP). The axis system used in C_{2v} calculations is illustrated in Structure II.[48] Full Cartesian coordinates and energies for the optimized geometries of each species are included in the Supporting Information (Tables S1−S10).

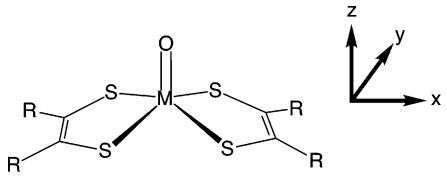

II

VDEs of the $[M^{IV}O(mnt)_2]^{2-}$ centers were calculated by the ΔSCF method, i.e., the difference in energy between the parent dianion and the ground state of the product anion with its geometry fixed at that of the parent species.[49] ADEs were calculated by the same procedure except the geometry of the product anion was allowed to relax.

The excited states of the anions $[M^{V}O(mnt)_2]^-$ and $[M^{V}O(bdt)_2]^-$ were predicted using time-dependent density functional theory (TD-DFT) as implemented in the Gaussian 98 program.[45] A sufficient number of excited states were calculated at each of the relevant geometries of the product anions to encompass the lowest lying ligand−metal charge-transfer transitions that are relevant to the present study. Theoretical predictions for the position of photoelectron bands were obtained from the difference in energy between the parent dianions $[M^{IV}O(mnt)_2]^{2-}$ and the ground and excited states of the product anions $[MO(mnt)_2]^-$.[50]

Results

Photoelectron Spectroscopy of $[M^{IV}O(mnt)_2]^{2-}$ (M = Mo, W). PES spectra recorded at four different photon wavelengths for the Mo and W systems are shown in Figures 1and 2, respectively. The ADE of the threshold peak and the VDEs of all the labeled features for both complexes are listed in Table 1. For the molybdenum species, three well-separated bands (X, A, B) were observed at lower binding energies in the 157-nm spectrum (Figure 1d). The separation between bands X and A is ∼0.69 eV. Additional overlapping features were observed at higher binding energies, and seven of these are labeled in Figure 1 for later discussion (bands C−I). The lower photon energy spectra show fewer spectral features but better resolution. Bands G−I were not observed in the 193-nm spectrum (Figure 1c) due to the repulsive coulombic barrier (RCB), discussed in more detail below. The relative intensity of band A showed a strong dependence upon photon energy (Figure 1c,d). Band C is absent

(44) $[Mo^{IV}O(mnt)_2]^{2-}$ is approximately 1.1 V more difficult to oxidize in solution than the parent member of the series $[Mo^{IV}O(edt)_2]^{2-}$ (edt = 1,2-ethenedithiolato). See ref 11 for a comparison of the redox potentials of a variety of $[MoO(dithiolene)_2]^{2-}$ centers. Some $[MoO(dithiolene)_2]^{2-}$ dianions are expected to be unstable in the gas phase. For example, calculations predicted that the VDE of $[Mo^{IV}O(bdt)_2]^{2-}$ is approximately −0.7 eV, suggesting that this dianion is likely to be thermodynamically unstable with respect to electron autodetachment. This is true for many multiply charged anions that are stabilized in solution by solvation. See, for example: Dreuw, A.; Cederbaum, L. S. *Chem. Rev.* **2002**, *102*, 181 and ref 51.

(45) Frisch, M. J.; Trucks, G. W.; Schlegel, H. B.; Scuseria, G. E.; Robb, M. A.; Cheeseman, J. R.; Zakrzewski, V. G.; Montgomery, J. A., Jr.; Stratmann, R. E.; Burant, J. C.; Dapprich, S.; Millam, J. M.; Daniels, A. D.; Kudin, K. N.; Strain, M. C.; Farkas, O.; Tomasi, J.; Barone, V.; Cossi, M.; Cammi, R.; Mennucci, B.; Pomelli, C.; Adamo, C.; Clifford, S.; Ochterski, J.; Petersson, G. A.; Ayala, P. Y.; Cui, Q.; Morokuma, K.; Malick, D. K.; Rabuck, A. D.; Raghavachari, K.; Foresman, J. B.; Cioslowski, J.; Ortiz, J. V.; Stefanov, B. B.; Liu, G.; Liashenko, A.; Piskorz, P.; Komaromi, I.; Gomperts, R.; Martin, R. L.; Fox, D. J.; Keith, T.; Al-Laham, M. A.; Peng, C. Y.; Nanayakkara, A.; Gonzalez, C.; Challacombe, M.; Gill, P. M. W.; Johnson, B. G.; Chen, W.; Wong, M. W.; Andres, J. L.; Head-Gordon, M.; Replogle, E. S.; Pople, J. A. *Gaussian 98*, revision A.7; Gaussian, Inc.: Pittsburgh, PA, 1998.

(46) Schaftenaar, G.; Noordik, J. H. *J. Comput.-Aided Mol. Des.* **2000**, *14*, 123−134.

(47) Stevens, W. J.; Krauss, M.; Basch, H.; Jaisen, P. *Can. J. Chem.* **1992**, *70*, 612−630.

(48) The coordinate system of C_{2v} symmetry is rotated 45° relative to that for C_{4v} point symmetry. C_{2v} symmetry labels are used throughout as these are appropriate for the $[M^{IV}O(mnt)_2]^{2-}$ centers of the present study. This results in the lowest-energy metal-based orbital being denoted $d_{x^2-y^2}$, while the equivalent orbital in C_{4v} symmetry is denoted d_{xy}.

(49) Rienstra-Kiracofe, J. C.; Tschumper, G. S.; Schaefer, H. F., III; Nandi, S.; Ellison, G. B. *Chem. Rev.* **2002**, *102*, 231−282.

(50) TD-DFT has been used previously to assign photoelectron spectra. For some recent examples, see: (a) Li, X.; Kiran, B.; Li, J.; Zhai, H.-J.; Wang, L.-S. *Angew. Chem., Int. Ed.* **2002**, *41*, 4786−4789. (b) Dai, B.; Deng, K.; Yang, J.; Zhu, Q. *J. Chem. Phys.* **2003**, *118*, 9608−9613. (c) Hirata, S.; Head-Gordon, M.; Szczepanski, J.; Vala, M. *J. Phys. Chem. A* **2003**, *107*, 4940−4951.

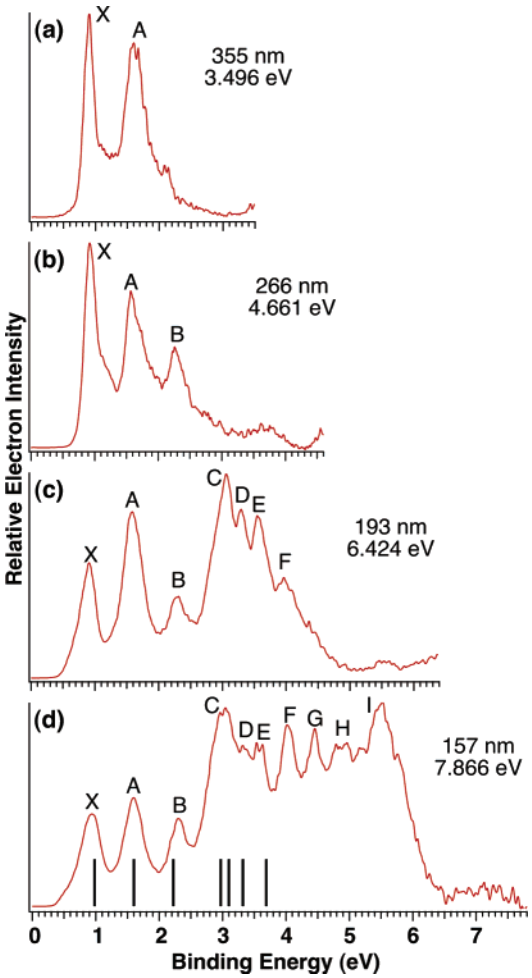

Figure 1. Photoelectron spectra of $[Mo^{IV}O(mnt)_2]^{2-}$ at (a) 355, (b) 266, (c) 193, and (d) 157 nm. The solid bars in (d) represent the theoretically predicted position of the VDEs of the photoelectron bands (see text and Table 5).

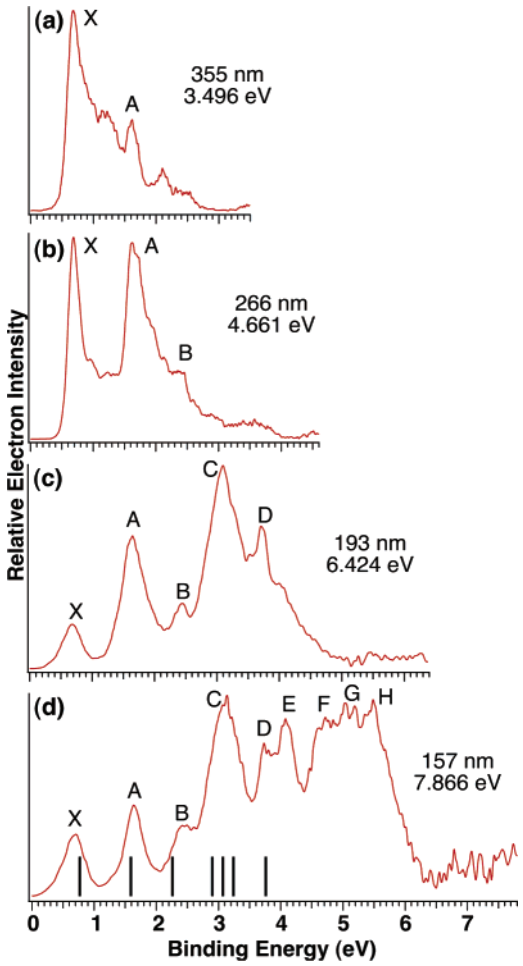

Figure 2. Photoelectron spectra of $[W^{IV}O(mnt)_2]^{2-}$ at (a) 355, (b) 266, (c) 193, and (d) 157 nm. The solid bars in (d) represent the theoretically predicted position of the VDEs of the photoelectron bands (see text and Table 5).

in the 266-nm spectrum due to the RCB (Figure 1b), while only bands X and A are observed in the 355-nm spectrum (Figure 1a). The overall spectral patterns of $[W^{IV}O(mnt)_2]^{2-}$ are qualitatively similar (Figure 2). The threshold band X has a lower binding energy compared with that of $[Mo^{IV}O(mnt)_2]^{2-}$ (0.69 vs 0.91 eV, respectively), while the positions of other spectral features are relatively unchanged. This results in a larger energy gap (~0.95 eV) between bands X and A for $[W^{IV}O(mnt)_2]^{2-}$.

DFT Calculations. The geometries of $[M^{IV}O(mnt)_2]^{2-}$ were optimized under constrained C_{2v} point symmetry, and the calculated structural parameters compared well with those determined experimentally by X-ray crystallography (Tables S11, S12).[11,18] Absolute and relative orbital energies for the seven highest-energy occupied molecular orbitals of both species are given in Table 2. These are illustrated for the molybdenum case in Figure 3, while the tungsten case is qualitatively similar (Figure S2). The HOMOs of $[M^{IV}O(mnt)_2]^{2-}$ were predicted to be of a_1 symmetry and based upon the metal $d_{x^2-y^2}$ orbital (Structure II, Figure 3, Table 2). The next six molecular orbitals arise from different linear combinations of ligand sulfur 3p atomic orbitals (SALCs) symmetry-adapted for interaction with M and O atomic orbitals. Some of these also feature a contribution from C 2p atomic orbitals involved in the C═C bond of the dithiolene unit (π or π^*). Orbitals consisting of sulfur 3p orbitals that are approximately orthogonal to the Mo−S bond vectors are denoted S(π) (e.g., HOMO−1; Figure 3), while those consisting of sulfur 3p orbitals that are directed approximately along the Mo−S bond vectors are denoted S(σ) (e.g., HOMO−4; Figure 3).[28,29] In agreement with previous theoretical studies, the majority of S(π) orbitals are predicted to lie at higher energies than the S(σ) orbitals.[27,32] The lowest-energy S(π) and highest-energy S(σ) orbitals have similar energies (Table 2).

Table 1. Experimental Adiabatic (ADE) and Vertical (VDE) Detachment Energies for the $[M^{IV}O(mnt)_2]^2$ Anions[a]

	band	$[MoO(mnt)_2]^{2-}$	$[WO(mnt)_2]^{2-}$
ADE		0.78(2)	0.54(2)
VDE	X	0.91(2)	0.69(2)
	A	1.60(2)	1.64(2)
	B	2.30(2)	2.44(4)
	C	3.06(4)	3.11(4)
	D	3.30(4)	3.73(6)
	E	3.57(4)	4.08(6)
	F	4.03(6)	4.73(8)
	G	4.45(6)	5.10(8)
	H	4.88(8)	5.49(8)
	I	5.50(8)	

[a] The numbers in parentheses represent the uncertainty in the last digit.

Table 2. Calculated Molecular Orbitals from Spin-Restricted DFT Calculations for the $[M^{IV}O(mnt)_2]^{2-}$ Anions[a]

	$[MoO(mnt)_2]^{2-}$			$[WO(mnt)_2]^{2-}$		
MO no.	*E*	Δ*E*	description	*E*	Δ*E*	description
82	0.23	0.00	a_1 Mo($d_{x^2-y^2}$)	0.51	0.00	a_1 W($d_{x^2-y^2}$)
81	−0.01	−0.24	b_1 S(π)	−0.07	−0.57	b_1 S(π)
80	−0.68	−0.91	a_1 S(π)	−0.78	−1.29	a_1 S(π)
79	−1.38	−1.61	a_2 S(π)	−1.40	−1.90	a_2 S(π)
78	−1.47	−1.70	b_2 S(σ)	−1.52	−2.02	b_2 S(σ)
77	−1.70	−1.93	b_2 S(π)	−1.70	−2.20	b_2 S(π)
76	−2.07	−2.30	b_1 S(σ)	−2.19	−2.70	b_1 S(σ)

[a] Absolute (*E*, eV) and relative (Δ*E*, eV) orbital energies are listed.

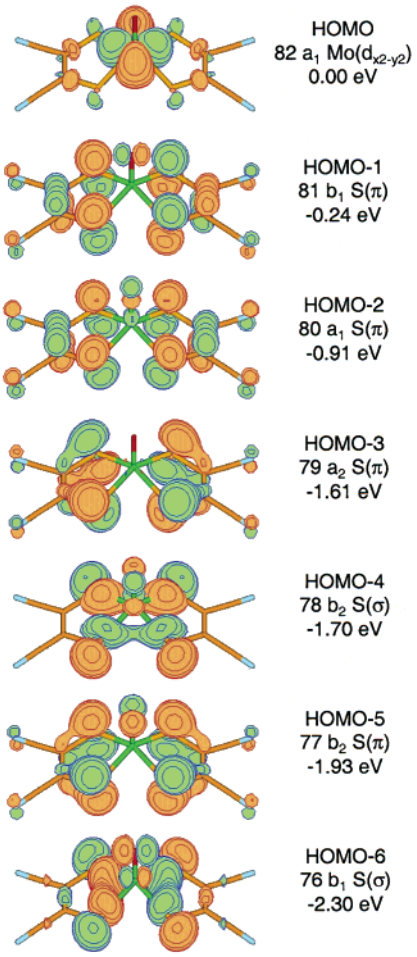

Figure 3. DFT MO contour plots for $[Mo^{IV}O(mnt)_2]^{2-}$ (contour cutoff value = 0.04). Orbital symmetries (based on C_{2v} point symmetry) and orbital energies (eV) relative to the HOMO are listed.

The products of electron detachment from the ground-state singlet species $[M^{IV}O(mnt)_2]^{2-}$ are singly charged anions $[MO(mnt)_2]^-$. The spin selection rule ($\Delta S = \pm 1/2$) suggests that only doublet configurations of the product anions are likely to be accessible. Spin-unrestricted DFT calculations were carried out for the product anions with their geometry fixed at that of the parent dianion. The seven highest-energy-occupied α- and β-spin orbitals for the ground state of the molybdenum anion $[MoO(mnt)_2]^-$ are given in Table 3. The tungsten case is qualitatively similar (Figure S4). These calculations suggested that the single unpaired electron in these anions resides in the a_1 $d_{x^2-y^2}$-based molecular orbital that corresponds to the doubly occupied HOMO of the parent dianions. These orbitals are the lowest-energy-unoccupied β-spin orbitals, and the corresponding α-spin orbitals are occupied. The latter are at lower energies than the highest-lying α-spin ligand-based orbitals. A similar mixed-level scheme has been observed previously in spin-unrestricted DFT calculations on related species.[29,32] The lowering in energy of the α-spin $d_{x^2-y^2}$ orbitals was attributed to spin-polarization.

Table 3. Calculated α- and β-Spin Orbitals from Spin-Unrestricted DFT Calculations on $[Mo^{V}O(mnt)_2]^-$ at the Geometry of $[Mo^{IV}O(mnt)_2]^{2-}$[a]

	α-spin orbitals			β-spin orbitals		
MO no.	*E*	Δ*E*	description	*E*	Δ*E*	description
82	−3.84	0.0	b_1 S(π)	−2.20	+1.64	a_1 Mo($d_{x^2-y^2}$)[b]
81	−4.49	−0.65	a_1 S(π)	−3.84	0.0	b_1 S(π)
80	−5.22	−1.38	a_2 S(π)	−4.47	−0.63	a_1 S(π)
79	−5.38	−1.54	a_1 Mo($d_{x^2-y^2}$)	−5.23	−1.38	a_2 S(π)
78	−5.52	−1.68	b_2 S(σ)	−5.47	−1.63	b_2 S(σ)
77	−5.58	−1.74	b_2 S(π)	−5.61	−1.76	b_2 S(π)
76	−6.16	−2.32	b_1 S(σ)	−6.14	−2.30	b_1 S(σ)

[a] Absolute (E, eV) and relative (Δ*E*, eV) orbital energies are listed. [b] Vacant.

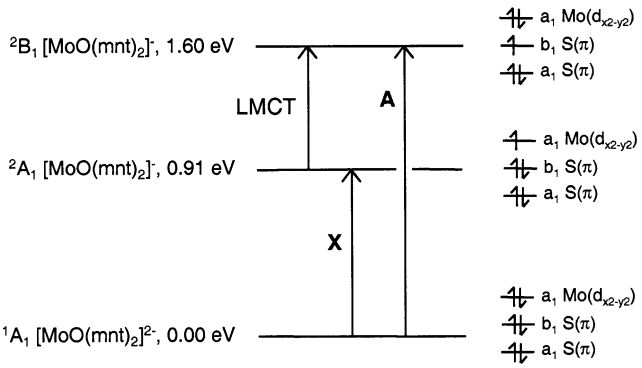

Figure 4. One-electron model indicating the relationship between the photodetachment bands X and A, and the lowest-energy LMCT transition of $[Mo^{V}O(mnt)_2]^-$. Energies (eV) are relative to the ground state of the parent dianion, $[Mo^{IV}O(mnt)_2]^{2-}$. The separation between bands X and A corresponds to the energy of the first LMCT transition of $[Mo^{V}O(mnt)_2]^-$, estimated to be 0.69 eV.

Excited states of the anions $[MO(mnt)_2]^-$ were accessed by electron detachment from ligand-based molecular orbitals of $[M^{IV}O(mnt)_2]^{2-}$. Within the single particle approximation, these excited states are equivalent to those arising from promotion of a single electron from a doubly occupied ligand-based orbital of $[M^{V}O(mnt)_2]^-$ to the singly occupied metal-based $d_{x^2-y^2}$ orbital (Figure 4). The relevant ligand-based orbitals from which detachment occurs correspond to the four S(π) and the two highest-energy S(σ) orbitals (Figure 3). The separation between band X and bands at higher binding energies corresponds to the energy of ligand−metal charge-transfer transitions of the product anions $[M^{V}O(mnt)_2]^-$ (e.g., Figure 4). As a consequence of the vertical nature of the electron detachment process, these ligand−metal charge-transfer data are accessed at the geometry of the parent $[Mo^{IV}O(mnt)_2]^{2-}$ anions. As a further result of the nature of the detachment process, excited states arising from electronic transitions to molecular orbitals that are vacant in the parent dianion should not be observed.

TD-DFT calculations were used to estimate the energies of the relevant excited states and also the oscillator strengths for the transitions of lowest energy to assist comparison with

Table 4. Comparison of Experimental[a] and Theoretical[b] β-Spin MO → 82 $d_{x^2-y^2}$ Transition Energies for $[M^{V}O(mnt)_2]^-$ Anions[c]

	$[Mo^{V}O(mnt)_2]^-$				$[W^{V}O(mnt)_2]^-$			
MO	band	exptl	calcd	$f_{calcd} \times 10^3$	band	exptl	calcd	$f_{calcd} \times 10^3$
81 b_1 S(π)	A	0.69	0.62	0.0	A	0.95	0.82	0.0
80 a_1 S(π)	B	1.39	1.24	0.1	B	1.75	1.49	0.1
79 a_2 S(π)	C	1.90−2.20	1.98	0.0	C	2.15−2.60	2.13	0.0
78 b_2 S(σ)	C	1.90−2.20	2.11	2.1	C	2.15−2.60	2.30	2.3
77 b_2 S(π)	D	2.39	2.33	0.0	C	2.15−2.60	2.47	0.0
76 b_1 S(σ)	E	2.66	2.71	0.0	D	3.04	2.99	0.0

[a] Experimental vertical transition energies, estimated by the separation from band X (Table 1). [b] Calculated vertical transition energies and oscillator strengths (f_{calcd}) were predicted by TD-DFT calculations at the geometry of $[M^{IV}O(mnt)_2]^{2-}$. [c] Predicted oscillator strengths (f_{calcd}) are included.

Table 5. Experimental and Calculated Vertical Detachment Energies (VDE) and Band Assignments for Photoelectron Spectra of the $[M^{IV}O(mnt)_2]^{2-}$ Centers

	$[Mo^{IV}O(mnt)_2]^{2-}$				$[W^{IV}O(mnt)_2]^{2-}$			
band	exptl[a]	calcd[b]	assignment	band	exptl[a]	calcd[b]	assignment
X	0.91(2)	0.98	$[a_1\ Mo(d_{x^2-y^2})]^{-1}$	X	0.69(2)	0.77	$[a_1\ W(d_{x^2-y^2})]^{-1}$
A	1.60(2)	1.60	$[b_1\ S(\pi)]^{-1}$	A	1.64(2)	1.59	$[b_1\ S(\pi)]^{-1}$
B	2.30(2)	2.22	$[a_1\ S(\pi)]^{-1}$	B	2.44(4)	2.26	$[a_1\ S(\pi)]^{-1}$
C	3.06(4)	2.97	$[a_2\ S(\pi)]^{-1}$	C	3.11(4)	2.90	$[a_2\ S(\pi)]^{-1}$
		3.10	$[b_2\ S(\sigma)]^{-1}$			3.07	$[b_2\ S(\sigma)]^{-1}$
D	3.30(4)	3.32	$[b_2\ S(\pi)]^{-1}$			3.24	$[b_2\ S(\pi)]^{-1}$
E	3.57(4)	3.69	$[b_1\ S(\sigma)]^{-1}$	D	3.73(6)	3.76	$[b_1\ S(\sigma)]^{-1}$

[a] The numbers in parentheses represent the uncertainty in the last digit. [b] VDEs were calculated from the difference in energy between the parent dianions and the ground and excited states of the product anions with their geometries fixed at that of the parent species.

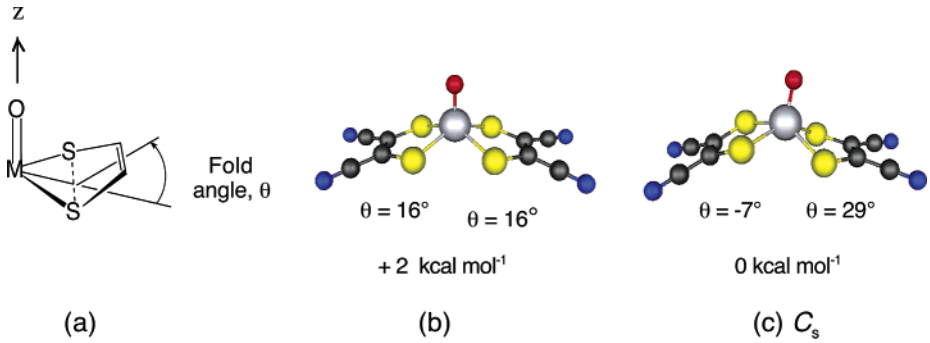

Figure 5. (a) Definition of the dithiolene fold angle. (b) $[Mo^{V}O(mnt)_2]^-$ optimized under C_{2v} point symmetry. (c) $[Mo^{V}O(mnt)_2]^-$ optimized under C_s point symmetry.

electronic absorption data. Oscillator strengths cannot be derived from the photodetachment spectra. The predicted transition energies for promotion to the singly occupied $d_{x^2-y^2}$ orbital are detailed in Table 4 and compared with experimental values derived from the separation between bands X and bands at higher binding energies. These data represent the vertical excitation energies of $[M^{V}O(mnt)_2]^-$ centers with their geometry fixed at that of the C_{2v} point symmetry of the parent anions $[M^{IV}O(mnt)_2]^{2-}$. Although not relevant to the present experiments, the calculated oscillator strengths of these transitions are also included in Table 4. The lowest-energy ligand-field transitions are predicted to occur at approximately 2 eV for both species (data not shown). These transitions are not accessible in the present experiments and are not discussed further.

VDEs were predicted theoretically from the difference in energy between the ground state of parent $[M^{IV}O(mnt)_2]^{2-}$ and the ground and excited states of product $[M^{V}O(mnt)]^-$. These are listed in Table 5 and compared with experimental values. ADEs of the anions $[M^{IV}O(mnt)_2]^{2-}$ were estimated by allowing the geometry of the product anions $[M^{V}O(mnt)_2]^-$ to relax from C_{2v} to C_s point symmetry (Figure 5). Calculations predicted ADEs of 0.87 and 0.68 eV for $[Mo^{IV}O(mnt)_2]^{2-}$ and $[W^{IV}O(mnt)_2]^{2-}$, respectively, compared with experimental estimates of 0.78 and 0.54 eV (Table 1).

Discussion

Repulsive Coulombic Barrier and Intramolecular Coulombic Repulsion. The disappearance of higher binding energy features in the spectra recorded at lower photon energies (Figures 1 and 2) is a direct consequence of the RCB.[51−53] In multiply charged anions, this arises from the superposition of short-range attraction and long-range electron repulsion and is equivalent to the intramolecular coulombic repulsion derived from the excess negative charges in these species.[54] The present systems $[MO(mnt)_2]^{2-}$ were chosen because preliminary considerations indicated that the electron-withdrawing cyanide substituents would ensure positive electron affinities and stable dianions in the gas phase. This contrasts with the 1,2-ethene- and 1,2-benzene-dithiolato derivatives that are predicted to be unstable.[44]

The effect of the RCB can be detected by comparison of spectra recorded at different photon energies. For example, for

(51) Wang, L. S.; Wang, X. B. *J. Phys. Chem. A* **2000**, *104*, 1978.
(52) Wang, X. B.; Yang, X.; Wang, L. S. *Int. Rev. Phys. Chem.* **2002**, *21*, 473.
(53) Wang, X. B.; Ding, C. F.; Wang, L. S. *Phys. Rev. Lett.* **1998**, *81*, 3351.
(54) Wang, L. S.; Ding, C. F.; Wang, X. B.; Nicholas, J. B. *Phys. Rev. Lett.* **1998**, *81*, 2667.

the molybdenum case, bands G to I were absent in the 193-nm spectrum (Figure 1c), despite the photon energy exceeding the VDEs of these bands. Similarly, bands C to F were absent in the 266-nm spectrum (Figure 1b). The magnitude of the RCB can be estimated from the spectral cutoff of the photon-energy-dependent spectra. The VDE of band F for $[MoO(mnt)_2]^{2-}$ was measured as 4.03 eV from the 157-nm spectrum (Figure 1d). This band was shifted to a slightly lower value in the 193-nm spectrum, and its relative intensity was decreased (Figure 1c). This suggested that the 193-nm photon was near or slightly below the RCB of band F,[55] allowing an estimate of the barrier height as ~2.4 eV (6.42−4.03 eV). The spectral cutoff for the 266-nm spectrum is then estimated to be ~2.3 eV (4.66−2.4 eV), and experimentally, there are no spectral features beyond 2.3 eV (Figure 1b). A similar spectral cutoff of 1.1 eV was predicted for the 355-nm spectrum (3.5−2.4 eV) but band A appeared at 1.6 eV. This may be due to the high intensity of this band at 355 nm and to electron tunneling. Using the same procedure, we estimated the RCB to be 2.3 eV for $[W^{IV}O(mnt)_2]^{2-}$, very similar to that derived for $[Mo^{IV}O(mnt)_2]^{2-}$. This is consistent with similar structures imposing similar coulombic repulsion for each dianion.

Relationship between Adiabatic Detachment Energies and Oxidation Potentials. Electron detachment in the gas phase may be compared to one-electron oxidation in solution. As discussed below, the X features in the photoelectron spectra (Figures 1 and 2) correspond to removing an electron from the doubly occupied metal-based $d_{x^2-y^2}$ HOMO of each species. The ADE of $[W^{IV}O(mnt)_2]^{2-}$ is 0.24 eV lower than that of $[Mo^{IV}O(mnt)_2]^{2-}$ (Table 1), while in acetonitrile solution, the tungsten system is 0.20 eV more easily oxidized than the molybdenum congener.[17,18] Thus, ADEs in the gas-phase track oxidation potentials in solution, consistent with solvation effects being similar for dianions of similar structure.

The width of the first detachment feature, i.e., the difference in energy between the VDE and the ADE of band X, provides a measure of the intrinsic reorganization energy of the detachment event.[56] These were measured as 0.13 and 0.15 eV for $[Mo^{IV}O(mnt)_2]^{2-}$ and $[W^{IV}O(mnt)_2]^{2-}$, respectively, consistent with a relatively minor geometry change upon electron detachment. This is supported by the calculated values of 0.11 and 0.09 eV, respectively.

Spectral Assignment and Electronic Structures of $[M^{IV}O(mnt)_2]^{2-}$. The detachment features shown in the spectra of Figures 1 and 2 represent transitions from the ground state of the dianions to the ground and excited states of the corresponding singly charged anions (cf, Figure 4). Within the single-particle approximation (Koopmans' theorem), these features can be viewed as the ionization of electrons from the occupied molecular orbitals (MOs) of the parent anions $[M^{IV}O(mnt)_2]^{2-}$. Therefore, unlike other experimental methods based on electronic transitions from occupied MOs to empty or partially empty MOs, PES directly maps the energy levels of the occupied MOs, as well as providing valuable information about chemical bonding. Assignment of the photoelectron spectra (Figures 1 and 2, Table 5) was based upon the ordering of molecular orbitals in $[M^{IV}O(mnt)_2]^{2-}$ predicted from DFT calculations (Figure 3, Table 2) and the transition energies in $[M^{V}O(mnt)_2]^{-}$ estimated by TD-DFT calculations (Table 4). The three bands at lower binding energy (X, A, B) were well-resolved and could be assigned with confidence on the basis of their clear separation from neighboring bands and the good agreement between experiment and calculation. The assignment of bands at higher binding energies is more speculative due to the spectral density in this region.

Band X is expected to arise from electron detachment from the HOMO of the parent $[M^{IV}O(mnt)_2]^{2-}$ anions, predicted by DFT calculations to be the doubly occupied $d_{x^2-y^2}$-based orbital (Figures 3 and 4, Table 2). The electronic structure of species containing the $\{Mo^{IV}O\}^{2+}$ core is dominated by the strong field terminal oxo ligand, which destabilizes the Mo $4d_{xz}$, d_{yz}, and d_{z^2} orbitals relative to their d_{xy} and $d_{x^2-y^2}$ counterparts (Structure II).[48] This results in the $d_{x^2-y^2}$ orbital being lowest in energy and doubly occupied in these formal d^2 centers. Spin-unrestricted DFT calculations predicted that the ground states of product anions $[MO(mnt)_2]^{-}$ would contain the unpaired electron in the same orbital (Table 3). The assignment of band X to electron detachment from a metal-based orbital is consistent with the observed shift of this band to lower binding energy upon substitution of tungsten for molybdenum (Figures 1 and 2, Table 1). The vertical energy for ionization of an electron from the HOMO is the difference in energy between the parent dianion $[M^{IV}O(mnt)_2]^{2-}$ and the ground state of the product anion $[M^{V}O(mnt)_2]^{-}$, with the geometry of the product anion fixed at that of its parent dianion. DFT calculations predicted values of 0.98 eV for $[Mo^{IV}O(mnt)_2]^{2-}$ and 0.77 eV for $[W^{IV}O(mnt)_2]^{2-}$, in reasonable agreement with the experimental values (Table 5).

Band A was well-resolved in the spectra of both species. DFT calculations predicted the HOMO−1 of $[M^{IV}O(mnt)_2]^{2-}$ to be the highest-energy ligand-based S(π) molecular orbital, b_1 S(π) (Figure 3, Table 2). The calculations also suggested that this orbital was well-separated energetically from both the HOMO and HOMO−2 levels (Table 2). Consequently, band A is assigned to electron detachment from HOMO−1, the highest-energy ligand-based orbital. In contrast to band X, the position of band A was less sensitive to substitution of tungsten for molybdenum (Figures 1 and 2, Table 1), consistent with electron detachment from a ligand-based orbital.

The electronic configuration accessed in band A represents the first excited state of $[M^{V}O(mnt)_2]^{-}$ (Figure 4). The TD-DFT calculations suggested that the first excited state of the anions $[M^{V}O(mnt)_2]^{-}$ would arise from the electronic transition b_1 S(π) → a_1 $d_{x^2-y^2}$ (Table 4). Within the single particle approximation, the electronic configuration of this excited state corresponds to that accessed directly by electron detachment from the HOMO−1 of parent $[M^{IV}O(mnt)_2]^{2-}$ (Figure 4). Accordingly, the difference in energy between bands X and A corresponds to the energy of this transition. A theoretical prediction of the position of band A for both species was derived from the difference in energies calculated for parent $[M^{IV}O(mnt)_2]^{2-}$ and the first excited state of product $[M^{V}O(mnt)_2]^{-}$ (Figure 4). Band A was predicted to occur at approximately 1.60 eV for both the molybdenum and tungsten anions, in good agreement with the experimental values of 1.60 and 1.64 eV, respectively (Table 5).

Band B was also relatively insensitive to the nature of the metal, occurring at slightly higher binding energy for the

(55) Wang, X. B.; Ding, C. F.; Wang, L. S. *Phys. Rev. Lett.* **1998**, *81*, 3351.
(56) Wang, X. B.; Wang, L. S. *J. Chem. Phys.* **2000**, *112*, 6959.

tungsten species (Figures 1 and 2, Table 1). DFT calculations predicted the HOMO−2 of $[M^{IV}O(mnt)_2]^{2-}$ to be the second highest-energy S(π) orbital, a_1 S(π) (Figure 3). The electronic configuration accessed by electron detachment from this molecular orbital corresponds to the second excited state of $[M^{V}O(mnt)_2]^{-}$, arising from the transition a_1 S(π) → a_1 $d_{x^2-y^2}$. Calculations predicted band B to occur in the range 2.2−2.3 eV for both the molybdenum and tungsten anions, in reasonable agreement with the experimental values of 2.30 and 2.44 eV, respectively (Table 5).

Band C is considerably broader and more intense than the three bands at lower binding energies, and spectral density is also considerably higher in this region (Figures 1 and 2). A weaker feature labeled D is evident on the higher-energy shoulder of band C for the molybdenum species (Figure 1d), but no similar feature is resolved for the tungsten species (Figure 2d). The spectral density observed in the region of band C for both species is qualitatively supported by the DFT calculations which predicted that the HOMO−3, HOMO−4, and HOMO−5 lie within approximately 0.3 eV of each other (Table 2). The third, fourth, and fifth excited states of $[M^{V}O(mnt)_2]^{-}$ are predicted to occur at similar energies (Table 4). They arise, respectively, from transitions to the orbital a_1 $d_{x^2-y^2}$ from the orbitals a_2 S(π), b_2 S(σ), and b_2 S(π). These excited states would be accessed directly by electron detachment from the HOMO−3, HOMO−4, and HOMO−5 levels of the parent $[M^{IV}O(mnt)_2]^{2-}$ anions (Figure 3, Table 2). For the molybdenum case, the predicted band positions for detachment from the HOMO−3 and HOMO−4 correspond to the onset and center of band C, respectively (Figure 1, Table 5). The predicted band position for detachment from the HOMO−5 might be assigned to the shoulder labeled band D (Figure 1c,d). For the tungsten case, similar assignments are possible for detachment from the HOMO−3 and HOMO−4. However, a feature equivalent to that observed for the molybdenum congener on the higher binding energy side of band C (band D) is not resolved and is presumably contained within band C. Accordingly, for the tungsten case, band C is assigned to detachment from the HOMO−3, HOMO−4, and HOMO−5 levels of parent $[W^{IV}O(mnt)_2]^{2-}$ (Figure 2, Table 5).

The next accessible excited state is predicted to arise from the transitions b_1 S(σ) → a_1 $d_{x^2-y^2}$ (Table 4), giving rise to an electronic configuration that corresponds to that accessed directly by electron detachment from the HOMO−6 of parent $[M^{IV}O(mnt)_2]^{2-}$. These bands are predicted to occur in the range 3.7−3.8 eV for both the molybdenum and tungsten anions (Table 5). The theoretical values are in acceptable agreement with the experimental band positions of 3.57 and 3.73 eV.

Electronic Structure of the Anions $[M^{V}O(mnt)_2]^{-}$. Electron detachment from $[M^{IV}O(mnt)_2]^{2-}$ gave access to the ground and excited states of the anions $[M^{V}O(mnt)_2]^{-}$. Energy differences between spectral features provided estimates of the energies (but not the intensities) of ligand−metal charge-transfer transitions from S(π) and S(σ) molecular orbitals to the singly occupied $d_{x^2-y^2}$ orbital of product $[M^{V}O(mnt)_2]^{-}$. The latter has been demonstrated to be the HOMO in $[Mo^{V}OCl_4]^{-}$ and related species using EPR, absorption, MCD, and photoelectron spectroscopies, as well as calculations based on a variety of theoretical techniques.[32,57−64] A range of oxo-tetrathiolatomolybdenum(V) centers $[MoOS_4]^{-}$ (S_4 = tetrathiolato, bis(dithiolato), or bis(dithiolene)) centers have also been studied.[25−32]

The eight sulfur-based molecular orbitals S(π) and S(σ) lie directly below the $d_{x^2-y^2}$ HOMO and differ in their orientation with respect to the M−S bond vectors and to the valence d-orbitals of metals M (cf, Figure 3).[28,29] The remaining four SALCs derived from S 3p orbitals are involved in S−C(α) covalent bonding and lie at considerably lower energy. The relative energies of the S(π) and S(σ) levels and their interaction with metal-based orbitals depend strongly on the geometric structure of the MOS_4 core.[28,29,32] Important parameters include (i) the M−S−C angle, (ii) the O−M−S angle, (iii) the O−M−S−C dihedral angle, and (iv) the $MS_2-S_2C_2$ dihedral angle (dithiolene fold angle θ; Figure 5a).

The low-energy absorption features that are common to $[M^{V}OS_4]^{-}$ centers are proposed to arise from charge-transfer transitions from sulfur-based molecular orbitals to the singly occupied metal-based $d_{x^2-y^2}$ orbital. The effect of the O−Mo−S−C dihedral angle on the energy and intensity of these low-energy absorption features has been investigated in detail, both experimentally and theoretically.[28,29,32] As this angle is increased from 0 to 90° for monodentate thiolato ligands, the S(π) SALCs are rotated out of the $x-y$ plane, and their interaction with equatorial d orbitals is reduced. At the extreme of 90°, the S(π) SALCs cannot interact with Mo $4d_{x^2-y^2}$ or d_{xy} orbitals, and they lie at higher energy than the S(σ) orbitals. This observation is particularly important for dithiolene ligands, as this angle is maintained at approximately 85° due to the rigid backbone of the bidentate ligand. Interaction between dithiolene S(π) orbitals and the singly occupied Mo $4d_{x^2-y^2}$ orbital is expected to be minimal, and as a consequence, charge-transfer transitions from these higher-energy S(π) orbitals to Mo $4d_{x^2-y^2}$ are expected to have low oscillator strengths.[28,29] On this basis, the low-energy charge-transfer transitions observed for bis(dithiolene)oxomolybdenum(V) centers, including oxidized dimethyl sulfoxide reductase, have been assigned to S(σ) → Mo $4d_{x^2-y^2}$ transitions on the basis of their expected higher oscillator strengths.[27] The present study provides experimental estimates of a range of S → Mo $4d_{x^2-y^2}$ transitions (Table 4), but gives no information on experimental absorption intensities.

Ligand Folding in $[MO(S-S)_2]^{-}$ Anions. Dithiolene ligands may fold across the S···S vector as a consequence of interaction of a filled S(π) MO with the equatorial $d_{x^2-y^2}$ orbital (Figure 5a).[65,66] A strong correlation between fold angle θ and the occupancy of $d_{x^2-y^2}$ has been observed in a number of mono- and bis(dithiolene) complexes.[10,11,19,37,67−69] For example, in the series $Cp_2M(S-S)$, $\theta \approx 0-10°$ for d^2 centers but 40−50° for

(57) Gray, H. B.; Hare, C. R. *Inorg. Chem.* **1962**, *1*, 363−368.
(58) Hare, C. R.; Bernal, I.; Gray, H. B. *Inorg. Chem.* **1962**, *1*, 831−835.
(59) Sabel, D. M.; Gewirth, A. A. *Inorg. Chem.* **1994**, *33*, 148−156.
(60) Carducci, M. D.; Brown, C.; Solomon, E. I.; Enemark, J. H. *J. Am. Chem. Soc.* **1994**, *116*, 11856−11868.
(61) Weber, J.; Garner, C. D. *Inorg. Chem.* **1980**, *19*, 2206−2209.
(62) Deeth, R. J. *J. Chem. Soc., Dalton Trans.* **1991**, 1895−1900.
(63) Swann, J.; Westmoreland, T. D. *Inorg. Chem.* **1997**, *36*, 5348−5357.
(64) Nemykin, V. N.; Basu, P. *Inorg. Chem.* **2003**, *42*, 4046−4056.
(65) Lauher, J. W.; Hoffman, R. *J. Am. Chem. Soc.* **1976**, *98*, 1729.
(66) Flemming, B.; Strauch, P.; Reinhold, J. *Organometallics* **2003**, *22*, 1196−1202.
(67) For some examples of dithiolene ligand folding in $Cp_2M(S-S)$ complexes, see: (a) Guyon, F.; Fourmigué, M.; Audebert, P.; Amaudrut, J. *Inorg. Chim. Acta* **1995**, *239*, 117−124. (b) Fourmigué, M.; Lenoir, C.; Coulon, C.; Guyon, F.; Amaudrut, J. *Inorg. Chem.* **1995**, *34*, 4979−4985. (c) Guyon, F.; Fourmigue, M.; Clerac, R.; Amaudrut, J. *J. Chem. Soc., Dalton Trans.* **1996**, 4093−4098. (d) Domercq, B.; Coulon, C.; Fourmigue, M. A *Inorg. Chem.* **2001**, *40*, 371−378.

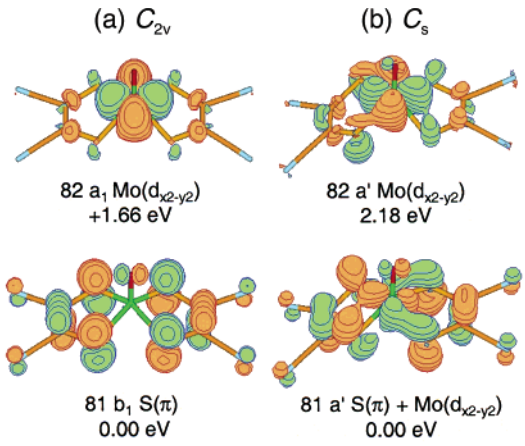

Figure 6. DFT MO contour plots (contour cutoff value = 0.04) of the frontier β-spin orbitals of $[Mo^{V}O(mnt)_2]^-$ at the geometry of: (a) C_{2v} point symmetry with equivalent dithiolene ligands and (b) C_s point symmetry with a folded dithiolene ligand. The highest-energy $d_{x^2-y^2}$-based orbitals are vacant in both cases, but the corresponding α-spin orbitals are occupied. Orbital symmetries and orbital energies relative to the HOMO are listed.

d^0 centers.[67] The d^1 centers exhibit a wider range $\theta \approx 0-40°$ intermediate between these extremes.[67]

The observed geometries of the parent anions $[M^{IV}O(mnt)_2]^{2-}$ are close to C_{2v} in the solid state with symmetric dithiolene ligands. The two equivalent ligands have fold angles $\theta \approx 12-13°$, consistent with $d_{x^2-y^2}$ being doubly occupied. The vertical nature of the detachment process indicates that the excited-state data for $[M^{V}O(mnt)_2]^-$ centers were also obtained at this geometry. However, some related d^1 $[M^{V}O(S-S)_2]^-$ species exhibit differential dithiolene ligand folding and a lower point symmetry (C_s).[10,11,19,70] Calculations on $[M^{V}O(mnt)_2]^-$ in the present work also predicted that C_s geometries with differentially folded dithiolene ligands would be favored slightly (~2 kcal mol^{-1}) over those of C_{2v} point symmetry (Figure 5b,c).

A comparison of the frontier β-spin orbitals for $[M^{V}O(mnt)_2]^-$ reveals the electronic origin of the differential ligand folding (Figure 6). The reduction from C_{2v} to C_s point symmetry allows a favorable covalent interaction between the vacant metal-based $d_{x^2-y^2}$ orbital (a_1 in C_{2v} point symmetry, a′ in C_s) and the highest-energy S(π) orbital (b_1 in C_{2v} point symmetry, a′ in C_s). These orbitals cannot mix under C_{2v} point symmetry. Accordingly, the two dithiolene ligands are predicted to fold in opposite directions (asymmetric folding; Figures 5c and 6). This effect has been observed experimentally in the equivalent bis(1,2-ethenedithiolato) system: while the d^2 complex features equivalent fold angles of +12°, the corresponding d^1 center exhibits different fold angles of +37 and +3°.[11] Similar observations have been reported for the series $[CpM(S-S)_2]^{n-}$ where variation of metal and charge has allowed a number of d^0, d^1, and d^2 examples to be characterized structurally.[68]

The present calculations predicted a single low imaginary frequency for the ligand folding vibration in both the $[M^{V}O(mnt)_2]^-$ centers constrained to C_{2v} geometry (e.g., Mo, −104 cm^{-1}; Figure 5b). This suggested that this geometry represents a transition state for ligand inversion between the two equivalent geometries of C_s point symmetry (Figure 5c). Barriers for ligand inversion are predicted to be low (e.g., Mo, ~2 kcal/mol), consistent with flat potential energy surfaces for ligand folding.[71] The geometries of these M^{V} transition states correspond closely to those of the parent centers $[M^{IV}O(mnt)_2]^{2-}$. The similarity of these geometries and the vertical nature of the detachment process suggested that the experimental data for $[M^{V}O(mnt)_2]^-$ (Table 4) were obtained at geometries very close to these transition states. Photoelectron spectroscopy has been used to access transition states previously.[33] For example, electron detachment from the radical anion of cyclooctatetraene ($COT^{\bullet-}$) accessed a planar geometry corresponding to the transition state between the equivalent "tub" geometries of neutral ground-state COT.[33c,d]

Effect of Ligand Folding on Charge-Transfer Transitions. The excited-state data for $[M^{V}O(mnt)_2]^-$ were accessed prior to ligand folding. Such folding would result in mixing of the frontier orbitals, changing their energies and composition (e.g., Figure 6). This aspect prompted a theoretical exploration of excited-state energies and oscillator strengths for $[M^{V}O(mnt)_2]^-$ centers at their lowest-energy geometries for both C_{2v} and C_s point symmetry. These calculations suggested that ligand folding would result in a large increase in intensity for a particular S(π) → $d_{x^2-y^2}$ transition (Tables S23−S26). However, detailed electronic or MCD experimental data are not available to test these predictions as the anion appears to disproportionate in solution.[17] Data are available for the related center $[Mo^{V}O(bdt)_2]^-$ (bdt = 1,2-benzenedithiolato).[3,26,27] Importantly, this anion has also been characterized structurally in the solid state and exhibited C_s geometry with one folded dithiolene ligand (θ = 29.5, 10.8°).[10]

The geometry of $[Mo^{V}O(bdt)_2]^-$ was optimized under the constraints of C_{2v} and C_s point symmetries. Again, a flat potential energy surface for ligand folding was predicted, with the C_{2v} geometry expected to correspond to the transition state for ligand inversion.[71] The C_s geometry was predicted to be only slightly more stable (1.3 kcal mol^{-1}). The predicted fold angles of θ = 32.6, −5.1° can be compared with the experimental values given above. Agreement is acceptable for the ligand with the larger fold angle, but a more significant deviation is observed for the second ligand. These discrepancies may reflect the influence of crystal packing and/or counterion effects in the solid state or the inability of the present theoretical technique to describe adequately this flat region of the potential energy surface. The frontier β-spin orbitals for $[Mo^{V}O(bdt)_2]^-$ at C_{2v} and C_s point symmetries are illustrated in Figure 7.

The lowest-energy electronic absorptions of $[Mo^{V}O(bdt)_2]^-$ and oxidized dimethyl sulfoxide reductase were assigned previously on the basis of electronic adsorption and MCD spectroscopies and DFT calculations on the related species $[Mo^{V}O(edt)_2]^-$ (edt = 1,2-ethenedithiolato).[27] The transition at ~1.7 eV (highest oscillator strength) was assigned to 79 b_2 S(σ)

(68) For some examples of dithiolene ligand folding in $CpM(S-S)_2$ complexes, see: (a) Guyon, F.; Lenoir, C.; Fourmigué, M.; Larsen, J.; Amaudrut, J. *Bull. Soc. Chim. Fr.* **1994**, *131*, 217−226. (b) Fourmigué, M.; Coulon, C. *Adv. Mater.* **1994**, *6*, 948−952. (c) Domercq, B.; Coulon, C.; Feneyrou, P.; Dentan, V.; Robin, P.; Fourmigué, M. *Adv. Funct. Mater.* **2002**, *12*, 359−366.

(69) For a discussion of dithiolene ligand folding in Tp*MoE(S−S) (Tp* = hydrotris(3,5-dimethyl-1-pyrazolyl)borate; E = O, NO), see: (a) Joshi, H. K.; Inscore, F. E.; Schirlin, J. T.; Dhawan, I. K.; Carducci, M. D.; Bill, T. G.; Enemark, J. H. *Inorg. Chim. Acta* **2002**, *337*, 275−286. (b) See also ref 37.

(70) Not all $[M^{V}O(S-S)_2]^-$ centers exhibit asymmetric dithiolene ligands. See, for example, $[M^{V}O(S_2C_2Me_2)_2]^-$, refs 12, 22.

(71) A similar flat potential energy surface is predicted for dithiolene folding in the d^1 centers $[Cp_2M(dmit)]^+$ (M = Mo, W; dmit = 2-thioxo-1,3-dithiole-4,5-dithiolate); see ref 67d.

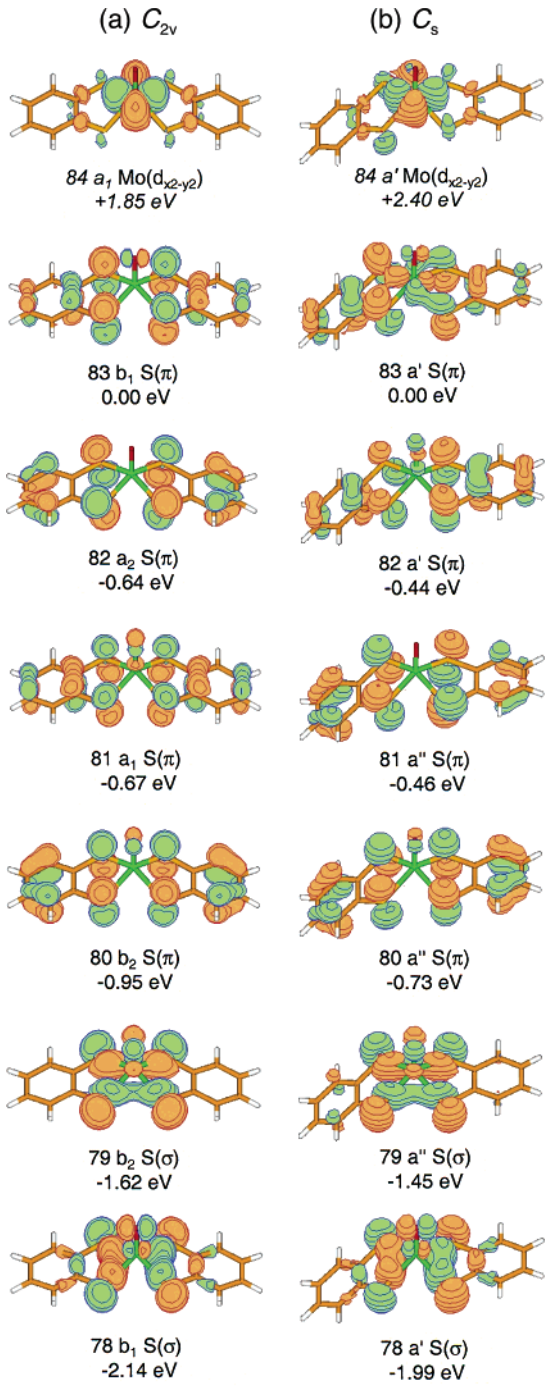

Figure 7. DFT MO contour plots (contour cutoff value = 0.04) of the frontier β-spin orbitals of $[Mo^{V}O(bdt)_2]^-$ at the geometry of: (a) C_{2v} point symmetry with equivalent dithiolene ligands and (b) C_s geometry with a folded dithiolene ligand. The highest-energy $d_{x^2-y^2}$-based orbitals are vacant in both cases, but the corresponding α-spin orbitals are occupied. Orbital symmetries and orbital energies relative to the HOMO are listed.

→ 84 a_1 Mo $d_{x^2-y^2}$ (Figure 7a; C_{2v} geometry).[72] This assignment was consistent with the expected higher oscillator strengths for S(σ) → Mo $d_{x^2-y^2}$ transitions compared with S(π) → Mo $d_{x^2-y^2}$ transitions, a consequence of the rigid dithiolene backbone restricting the O−Mo−S−C(α) dihedral angle to close to 90° and resulting in poor S(π)−Mo $d_{x^2-y^2}$ orbital overlap.[28,29]

(72) This b_2 S(σ) orbital was previously described as S_{ip}(nb) (ip = in-plane, nb = nonbonding). This orbital has been relabeled under the coordinate system and nomenclature of the present study.

Table 6. Calculated[a] Vertical Transition Energies and Oscillator Strengths (f_{calcd}) for β-Spin MO → 84 Mo $d_{x^2-y^2}$ Transitions of $[Mo^{V}O(bdt)_2]^-$ at Its Lowest-Energy Geometries of C_{2v} and C_s Point Symmetries

C_{2v} point symmetry			C_s point symmetry		
MO	energy (eV)	$f_{calcd} \times 10^3$	MO	energy (eV)	$f_{calcd} \times 10^3$
83 b_1 S(π)	0.86	0.8	83 a′ S(π) + $d_{x^2-y^2}$	1.24	0.8
81 a_1 S(π)	1.50	0.0	82 a′ S(π)	1.63	42.2
82 a_2 S(π)	1.53	0.0	81 a″ S(π)	1.72	4.7
80 b_2 S(π)	1.86	0.0	80 a″ S(π)	2.02	0.7
79 b_2 S(σ)	2.29	6.8	79 a″ S(σ)	2.51	2.8
78 b_1 S(σ)	2.75	0.4	79 a′ S(σ)	2.95	1.1

[a] TD-DFT calculations (see Experimental Section).

The excited states of $[M^{V}O(bdt)_2]^-$ centers were calculated by TD-DFT calculations at C_{2v} and C_s geometries. The six lowest-energy charge-transfer transitions for each case are detailed in Table 6. These correspond to transitions from occupied S(π) and S(σ) orbitals of β-spin to the vacant Mo $d_{x^2-y^2}$ orbital of β-spin (Figure 7). The only transition predicted to have significant oscillator strength at C_{2v} geometry is 79 b_2 S(σ) → 84 a_1 Mo $d_{x^2-y^2}$ (2.29 eV, $f_{calcd} = 6.8 \times 10^{-3}$; Table 6), consistent with the previous assignment.[27] However, the predicted transition energy is higher than the experimental absorption maximum at ∼1.7 eV.

For C_s geometry, a significant oscillator strength is predicted for the transition 82 a′ S(π) → 84 a′ Mo $d_{x^2-y^2}$ (1.63 eV, $f_{calcd} = 42.2 \times 10^{-3}$; Figure 7, Table 6). This results from increased orbital overlap and a large increase in electric dipole in the x direction (Structure II) as a consequence of ligand folding. The predicted transition energy is close to the experimental value of 1.7 eV and suggests a plausible alternative assignment. On the basis of a comparison of available experimental data, a similar alternative assignment also applies to the equivalent tungsten species (Tables S20 and S30, Figure S12).[3,19,26]

Conclusions

Photodetachment photoelectron spectroscopy was used to investigate the detailed electronic structure of the anions $[M^{IV}O(mnt)_2]^{2-}$ (M = Mo, W). The experiments provided information about the molecular orbital energy levels of these anions, as well as the ground and excited states of the product anions $[M^{V}O(mnt)_2]^-$. Detachment features were assigned on the basis of DFT calculations. The first feature (band X; Figures 1 and 2) was assigned to detachment from the metal-based $d_{x^2-y^2}$ HOMO. This assignment was consistent with the observed shift of this band to lower binding energy upon substitution of tungsten for molybdenum. Bands at higher binding energies were assigned to detachment from S(π) and S(σ) molecular orbitals. These assignments were consistent with these bands being less sensitive to substitution of the metal.

The separation between band X and bands at higher binding energies allowed estimation of the energies of ligand−metal charge-transfer transitions of the product anions $[M^{V}O(mnt)_2]^-$. These data correspond to the vertical transition energies of $[M^{V}O(mnt)_2]^-$ with their geometries fixed at the idealized C_{2v} point symmetry of the parent species $[M^{IV}O(mnt)_2]^{2-}$. However, calculations and available solid-state structures suggested that such species might relax to C_s geometries with differentially folded dithiolene ligands. Theoretical calculations indicated a low barrier to ligand inversion and that the intensity of certain

charge-transfer transitions in $[Mo^{V}O(S-S)]^{-}$ species depends dramatically on the geometric conformation of the ligand. For $[Mo^{V}O(bdt)_2]^{-}$ (and for oxidized dimethyl sulfoxide reductase by extension), an assignment a′ S(π) → a′ Mo $d_{x^2-y^2}$ is proposed for C_s geometry, a consequence of a predicted increase in intensity of 2 orders of magnitude as a result of dithiolene ligand folding (Table 6). This contrasts with the previous assignment S(σ) → Mo $d_{x^2-y^2}$, assuming C_{2v} geometry.[27]

Dithiolene ligand folding arises from interaction between the singly occupied or vacant equatorial metal-based orbital (HOMO; $d_{x^2-y^2}$; a_1 in C_{2v}, a′ in C_s) and the least stable occupied sulfur-based orbital (HOMO−1; S(π); b_1 in C_{2v}, a′ in C_s). The interaction depends on this S(π) orbital being of correct symmetry to interact with the $d_{x^2-y^2}$ orbital upon ligand folding and reduction to lower C_s point symmetry. The relative energies of the S(π) orbital manifold are affected by the presence of the C═C unit of the dithiolene ligand, as CC π or π* character can be mixed into the S(π) orbitals. The presence of this unsaturated bond in dithiolene ligands results in the least stable S(π) orbital being of the correct symmetry to interact with $d_{x^2-y^2}$. In contrast, the highest-energy ligand-based orbital of saturated dithiolato ligands is of incorrect symmetry to mix with $d_{x^2-y^2}$, and thus this orbital interaction does not occur.[73] This is of particular importance considering the presence of the dithiolene ligands in the Mo and W enzymes (Structure I).

Dithiolene ligand folding has been proposed to play an important role in the enzymatic cycles by coupling the S(π) orbitals of the pterin ligand into the redox-active metal-based orbital.[37] Such coupling may modulate redox properties and provide a tunable conduit for electron transfer between the metal center and its redox partners. This proposal is supported by the present study which demonstrates that barriers to ligand folding are low and that folding significantly affects the electronic structure of M^{V}-dithiolene units. In particular, the calculated oscillator strength of a S(π) → Mo $d_{x^2-y^2}$ charge-transfer transition in $[Mo^{V}O(bdt)_2]^{-}$ was increased by 2 orders of magnitude. Given that the electronic spectra of $[Mo^{V}O(bdt)_2]^{-}$ and the oxidized form of DMSO reductase are similar,[27,74] the sensitivity of the preferred dithiolene fold angle to occupation of the redox active $d_{x^2-y^2}$ orbital might play an important role in orientation of the dithiolene ligands during the course of the enzyme catalytic cycles. The fold angles in molybdenum enzymes of known structure vary in the range 6−33° (see ref 37).

Acknowledgment. Theoretical calculations were carried out using the legion cluster at the Melbourne Advanced Research Computing Centre (MARCC). T.W. acknowledges the receipt of an Australian Postgraduate Award and a Melbourne Abroad Travel Scholarship. L.Z. thanks the China Scholarship Council for financial support. R.A.J.O. thanks the Australian Research Council for financial support (Grant No. A00103008). The photoelectron spectroscopy experiments were supported by the National Institute of Health (GM-63555 to L.S.W.) and were carried out at W. R. Wiley Environmental Molecular Sciences Laboratory, a national scientific user facility sponsored by the U.S. Department of Energy's Office of Biological and Environmental Research and located at Pacific Northwest National Laboratory, which is operated for the DOE by Batelle.

Note Added in Proof. An open bicyclic form of the pterin cofactor has been observed in the crystal structure of nitrate reductase A from *Escherichia coli* (Bertero, M. G.; Rothery, R. A.; Palak, M.; Hou, C.; Lim, D.; Blasco, F.; Weiner, J. H.; Strynadka, N. C. *Nat. Struct. Biol.* **2003**, *10*, 681−687). This oxidized form and its reduced tricyclic partner are proposed as components of a redox switch to uncouple electron transfer from the molybdenum center in the xanthine dehydrogenase enzyme of *Rhodobacter capsulatus* (Aguey-Zinsou, K. F.; Bernhardt, P. V.; Leimkuhler, S. *J. Am. Chem. Soc.* **2003**, *125*, 15352−15358). Such major conformational changes would certainly affect the fold angles of the Mo(V) dithiolene units, supporting the conclusions of the present study.

Supporting Information Available: Cartesian coordinates and energies for the optimized geometries of each species (Tables S1−S10), structural parameters and comparison with experimental data (where available) for each of these cases (Tables S11−S20), calculated transition energies and oscillator strengths for the six lowest-energy S → M $d_{x^2-y^2}$ charge-transfer transitions for each of the M(V) species (Tables S21−S30), and DFT MO contour plots for the seven highest-energy occupied orbitals at the relevant geometry of each species (Figures S1−S12). This material is available free of charge via the Internet at http://pubs.acs.org.

JA039652O

(73) This is apparent by comparison of the ordering of S(π) orbitals of bis(dithiolene) and bis(dithiolato) centers both constrained to C_{2v} point symmetry. For example, the relative ordering of the S(π) orbitals of the bis(dithiolene) centers of the present study is different than those of the bis(dithiolato) center $[Mo^{V}O(SCH_2-CH_2S)]^{-}$; ref 29.

(74) Adams, B.; Smith, A.; Bailey, S.; McEwan, A. G.; Bray, R. C. *Biochemistry* **1999**, *38*, 8501.